Erik Jonsson School of Engineering and Computer Science

2014-02

# *Selectivity of Metal Oxide Atomic Layer Deposition on Hydrogen Terminated and Oxidized Si(001)-(2x1) Surface*

UTD AUTHOR(S): Roberto C. Longo, Stephen McDonnell, Don Dick, Robert M. Wallace, Yves J. Chabal and Kyeongjae Cho

©2014 American Vacuum Society

Find more research and scholarship conducted by the Erik Jonsson School of Engineering and Computer Science here. This document has been made available for free and open access by the Eugene McDermott Library. Contact libwebhelp@utdallas.edu for further information.

# Selectivity of metal oxide atomic layer deposition on hydrogen terminated and oxidized Si(001)-(2×1) surface

Roberto C. Longo, Stephen McDonnell, D. Dick, R. M. Wallace, Yves J. Chabal, James H. G. Owen, Josh B. Ballard, John N. Randall, and Kyeongjae Cho

Citation: Journal of Vacuum Science & Technology B **32**, 03D112 (2014); doi: 10.1116/1.4864619
View online: http://dx.doi.org/10.1116/1.4864619
View Table of Contents: http://scitation.aip.org/content/avs/journal/jvstb/32/3?ver=pdfcov
Published by the AVS: Science & Technology of Materials, Interfaces, and Processing

**Articles you may be interested in**

High-reliability passivation of hydrogen-terminated diamond surface by atomic layer deposition of Al2O3
J. Appl. Phys. **115**, 223711 (2014); 10.1063/1.4881524

In situ study of the role of substrate temperature during atomic layer deposition of HfO2 on InP
J. Appl. Phys. **114**, 154105 (2013); 10.1063/1.4825218

Atomic layer deposition of photoactive CoO/SrTiO3 and CoO/TiO2 on Si(001) for visible light driven photoelectrochemical water oxidation
J. Appl. Phys. **114**, 084901 (2013); 10.1063/1.4819106

Band offsets of Al2O3 and HfO2 oxides deposited by atomic layer deposition technique on hydrogenated diamond
Appl. Phys. Lett. **101**, 252108 (2012); 10.1063/1.4772985

Atomic layer deposited (TiO2)x(Al2O3)1x/In0.53Ga0.47As gate stacks for III-V based metal-oxide-semiconductor field-effect transistor applications
Appl. Phys. Lett. **100**, 062905 (2012); 10.1063/1.3684803

# Selectivity of metal oxide atomic layer deposition on hydrogen terminated and oxidized Si(001)-(2×1) surface


Roberto C. Longo,[a] Stephen McDonnell, D. Dick, R. M. Wallace, and Yves J. Chabal
*Department of Materials Science and Engineering, The University of Texas at Dallas, Richardson, Texas 75080*

James H. G. Owen, Josh B. Ballard, and John N. Randall
*Zyvex Labs, LLC, 1321 N. Plano Rd., Richardson, Texas 75081*

Kyeongjae Cho[b]
*Department of Materials Science and Engineering, The University of Texas at Dallas, Richardson, Texas 75080*



(Received 2 December 2013; accepted 24 January 2014; published 10 February 2014)



In this work, the authors used density-functional theory methods and x-ray photoelectron spectroscopy to study the chemical composition and growth rate of $HfO_2$, $Al_2O_3$, and $TiO_2$ thin films grown by *in-situ* atomic layer deposition on both oxidized and hydrogen-terminated Si(001) surfaces. The growth rate of all films is found to be lower on hydrogen-terminated Si with respect to the oxidized Si surface. However, the degree of selectivity is found to be dependent of the deposition material. $TiO_2$ is found to be highly selective with depositions on the hydrogen terminated silicon having growth rates up to 180 times lower than those on oxidized Si, while similar depositions of $HfO_2$ and $Al_2O_3$ resulted in growth rates more than half that on oxidized silicon. By means of density-functional theory methods, the authors elucidate the origin of the different growth rates obtained for the three different precursors, from both energetic and kinetic points of view. © *2014 American Vacuum Society*. [http://dx.doi.org/10.1116/1.4864619]


## I. INTRODUCTION

For more than two decades, the microelectronic industry has been dominated by an intense research toward an ever diminishing device feature size.[1,2] The industry has been using $SiO_2$ as the standard gate dielectric layer; however, with increased miniaturization, the fundamental limitations of this material will impede continued progress.[2,3] Therefore, two of the most critical issues are then the search for high-$\kappa$ replacement dielectric materials for $SiO_2$ and the development of deposition processes that will afford the control of film growth according to the particular needs. Atomic layer deposition (ALD) is a deposition technique based on alternating surface reactions that saturate the surface in each reaction cycle. It has recently received much attention due to its ability to obtain atomic layer control of growth.[4]

Understanding the nucleation of thin films deposited by ALD is important for many applications. In the case of metal oxide depositions on semiconducting substrates for use as gate insulators, the goal is generally to achieve high purity and conformal layers of a predictable thickness on a range of surface terminations. For this purpose, a number of studies have been carried out demonstrating the diverse nucleation properties of a range of metal oxide precursors on both hydrogen terminated and oxidized Si surfaces.[5–8] It has been previously shown using high-resolution transmission electron microscopy that $Al_2O_3$ deposits uniformly on hydrogen terminated surfaces when TMA [trimethylaluminum, $Al(CH_3)_3$] and $H_2O$ precursors[5] are used. However, deposition of $ZrO_2$ (Ref. 6) and $HfO_2$ (Ref. 8) using $ZrCl_4$ and $HfCl_4$ precursors resulted in island growth, indicating reduced reactivity with the hydrogen terminated surface. In two independent comparative studies of $HfO_2$ grown by ALD on both HF-last silicon and $SiO_2$ using the $HfCl_4$ precursor, which has an incubation period of about five cycles before growth begins on the hydrogen terminated Si surface,[8] it was shown that the growth rate does not become linear until after 30 cycles.[7] ALD can also be used for the deposition of metal contacts, and for such applications, a high level of selectivity can be useful to simplify patterning and allow deposition on in the desired areas. Using a $Ni(dmamb)_2$ precursor and $NH_3$ gas, Ni has been shown to deposit equally well on both Si and $SiO_2$. Area selective ALD (AS-ALD) could still be demonstrated by using a octadecyltrichlorosilane self-assembled monolayers to effectively prevent the Ni growth on selected areas.[9] This technique has been employed early to selectively deposit Co by AS-ALD on Si substrates,[10] after it had been shown to be effective for depositing patterned Pt for fuel cell applications.[11] In contrast to the metal oxide precursors which are generally found selectivity grow on $SiO_2$ and OH-terminated Si more than on hydrogen-terminated Si, Co depositions using the $^{t}$Bu-AllylCo$(CO)_3$ and dimethylhydrazine precursors was found to deposit preferentially on hydrogen-terminated Si with no detectable deposition on the OH-terminated Si surface.

The different aspects of the ALD reaction mechanisms and the thermochemistry of metal-oxide ALD growth on semiconductor surfaces have also been the focus of numerous theoretical investigations. Density-functional theory (DFT) has proven to be a useful tool to describe the early stages of molecular growth in semiconductor surfaces. In the particular case of


[a]Electronic mail: roberto.longo@utdallas.edu
[b]Electronic mail: kjcho@utdallas.edu

ALD reactions, there are several studies available in the literature, especially for $Al_2O_3$ (Refs. 12–17) and $TiO_2$ (Refs. 18–28) deposition on the Si(001) with different chemistry terminations, reporting the energetics and kinetic barriers of the different precursors for the metal-oxide ALD growth on the corresponding semiconductor surface. Most of them use cluster models of variable sizes to represent the surface, with the inherent limitations to this type of modeling work. Although there are few theoretical works about the activity of Hf precursors,[29–32] to our knowledge, no theoretical calculations of the kinetics of the deposition of the Hf molecular precursor used in our ALD experiments [tetrakis(dimethylamido)Hf, TDMA-Hf] has been reported.

In this paper, we use DFT to obtain the energetics and kinetic barriers of the first adsorption step of the three molecular precursors used in our ALD experiments for $Al_2O_3$, $HfO_2$, and $TiO_2$ (TMA, TDMA-Hf, and $TiCl_4$, respectively) deposition onto the hydrogen- and OH-terminated Si(001)-(2$\times$1) surface, to explain the different growth rates obtained in our experimental ALD work.

The organization of this paper is as follows. In Sec. II, we briefly describe the computational methods used in our calculations, whereas in Sec. III, we describe the experimental methodology. Our main results are presented and discussed in Sec. IV and, finally in Sec. V, we summarize our main conclusions.

## II. COMPUTATIONAL METHODS

The theoretical results presented in this work have been obtained with DFT calculations using plane wave basis sets and projector augmented wave (PAW) pseudopotentials, as implemented in the VASP code.[33,34] The electronic wave functions were represented by plane wave basis with a cutoff energy of 500 eV. We included the exchange correlation interactions by using the semilocal Perdew–Burke–Ernzerhof (PBE) functional of the generalized gradient approximation.[35] The PAW pseudopotentials represent the effect of the inner electrons. The $3p^6$ electrons of Ti were included explicitly as valence electrons in our calculations (together with $3d^2$ and $4s^2$). For Hf, we also included the semicore $5p^6$ electrons in the valence states (together with $5d^2$ and $6s^2$). In the case of Al, we used the $3s^2p^1$ valence configuration and, finally, for Cl, Si and O atoms, we used the common $3s^2p^5$, $3s^2p^2$ and $2s^2p^4$ valence states, respectively.

The unit cell of the ideal Si(100)-(2$\times$1) is made of two Si atoms per layer. In our simulations, we modeled the Si(100)-(2$\times$1) surface with a periodic slab containing six Si atomic layers, with the bottom Si layer passivated by two H atoms per Si atom, to account for the effects of the dangling bonds. As we are interested in explaining the different growth rates on a hydrogen passivated Si surface, the surface dimers are also passivated with hydrogen atoms. When corresponds, some of the surface hydrogen atoms were replaced by OH hydroxyl groups. Since VASP implements a periodic boundary conditions scheme, we introduced a vacuum region in the direction perpendicular to the slab of 15 Å of thickness, to avoid spurious interactions between replica images. We studied the initial adsorption step of the three different molecular precursors used in our experiments: TDMA-Hf, $Hf[N(CH_3)_2]_4$ (for $HfO_2$), TMA, $Al(CH_3)_3$ (for $Al_2O_3$), and $TiCl_4$ (for $TiO_2$). The three molecular precursors were initially adsorbed on the dimer-reconstructed side of the slab. To make their interaction sufficiently weak, we employed a (4$\times$4) unit cell with four dimers along the dimer row. Each Si layer comprises 16 atoms, for a total amount of 96 Si atoms in our model system. All the atoms, except the two bottom Si and hydrogen-passivating layers, were allowed to relax.

The kinetic barriers, transition states, and reaction paths were obtained using the climbing image-nudged elastic band method (CI-NEB).[36–38] This method allows us to obtain the minimum energy path (MEP) between a set of two different states. To do that, the reaction path is divided into a set of images "connected with a spring." During the relaxation, the initial and final states are kept frozen while the images move according to the constraint of the "elastic band." The MEP is then found when the components of the forces perpendicular to the "elastic band" vanish, the relative positions of the images and the barrier being determined by the parallel components of the forces.

In all cases, we used a $(3 \times 3 \times 1)$ $k$-point mesh (that gives us ten irreducible $k$ points) within the Monkhorst–Pack[39] scheme to ensure a convergence of 10 meV/unit cell. We performed structural relaxations without including any type of symmetry, to a tolerance of $10^{-4}$ eV in the total energy and 0.01 eV/Å in the forces on every atom, for both standard and CI-NEB structural minimizations.

## III. EXPERIMENTAL SET UP

For the experiments carried out in this work, Si (001) wafers were purchased from WRS Materials (Cz, $n$-type, double-side polished with a nominal resistivity of 1–5 Ω·cm) and cut into squares samples of approximately 1.0 cm $\times$ 1.0 cm. $SiO_2$ samples were prepared by immersing the sample in a piranha solution (98% $H_2SO_4$:30% $H_2O_2$, 3:1, v/v) at 80 °C for at least 30 min in order to remove hydrocarbons or metal contamination then immersing the sample into a diluted hydrofluoric acid (1:4, v/v with deionized water, DIW) for 1 min after which that removed the thermal oxide, after which, then immersing the sample into a piranha solution (98% $H_2SO_4$:30% $H_2O_2$, 3:1, v/v) at 80 °C for at least 15 min and rinsing with DIW that grew chemical $SiO_2$. Similarly, the Si-H surface was prepared by immersing the sample in a piranha solution (98% $H_2SO_4$:30% $H_2O_2$, 3:1, v/v) at 80 °C for at least 30 min then immersing the sample into a diluted hydrofluoric acid (1:4, v/v with DIW) for 1 min leaving behind a hydrogen-terminated Si(001) surface. After the samples were prepared, they were rinsed with DIW, dried with nitrogen, and loaded as quickly as possible into the ALD reactor.

The commercial ALD reactor used in this work was a hot walled Savannah 100 apparatus from Cambridge Nanotech Inc. Samples were loaded into the ALD reactor, which had a temperature of 150 °C and purged for 1 h in order to fully degas the samples. ALD cycles were then performed by pulsing (TMA, TDMA-Hf, or $TiCl_4$) for 0.1 s, purging for

60 s, pulsing $H_2O$ for 0.05 s, then purging for 60 s in preparation for the next ALD cycle. The purge time between precursor pulses was 60 s to maximize the removal of mobile precursors (noncovalently bonded) on the surface, which could otherwise still be present during the next precursor pulse. All purges were performed with flowing Ar at a pressure of $\leq 2 \times 10^{-1}$ mbar. To study the initial nucleation, thin films of <1 nm were deposited on $SiO_2$ and H-terminated Si simultaneously. To achieve this, $Al_2O_3$ were films grown using ten cycles of TMA/$H_2O$, $HfO_2$ films were grown using ten cycles of TDMA-Hf/$H_2O$, and $TiO_2$ films were grown using 25 cycles of $TiCl_4$/$H_2O$. Meaningful comparisons between experiment and DFT trends require equal thermal energy for each experiment, to this end the substrate temperatures were kept constant for all three depositions at 150 °C.

Following ALD, the samples were loaded into a multideposition/characterization system (base pressure $< 2\times10^{-11}$ mbar) described elsewhere.[40,41] XPS analysis was performed using a monochromatic Al K$\alpha$ x-ray source described previously.[42] For spectral analysis, the curve fitting software Aanalyzer was used.[43] Spectra were fitted with a Voigt line shape, and a Shirley background subtraction was used.

## IV. RESULTS AND DISCUSSION

### A. Results

To explain the large precursor dependence in the degree of selectivity found for $Al_2O_3$, $TiO_2$, and $HfO_2$ ALD deposition, we start by considering the reaction energetics and kinetics of each metal molecular precursor chemisorption. To that end, we have carried out DFT simulations of the first adsorption step of the three molecular precursors (TDMA-Hf, TMA, and $TiCl_4$) used in our ALD experiments, for metal-oxide growth on hydrogen-passivated and OH-terminated Si(001)-(2×1) surfaces. We first obtained the minimum energy configuration of the Si surface and the gas phase of the three molecules (isolated system), and then, the initial adsorption step, where the metal atom of the molecular precursor is bonded to one Si atom of the surface, and some molecular reaction products are detached from the surface. To obtain the kinetic energy barrier of the three reactions, we performed NEB calculations along the path followed by the three molecules in their reaction with the hydrogen-passivated or OH-terminated Si(100)-(2×1) surface.

Figure 1 shows the reaction path for the first adsorption step of the TMA and $TiCl_4$ molecular precursors on the hydrogen-passivated Si(001)-(2×1) surface, and Fig. 2 shows the reaction path undergone by the TDMA-Hf molecular precursor. If the surface is hydrogen-passivated, the Si dangling bonds are saturated and, consequently, the surface dimers are no longer buckled, as compared to the clean Si(001) surface. The hydrogen-termination hinders the chemisorption process, increasing the kinetic energy barriers of the chemisorption reactions. Comparing Figs. 1 and 2, one can note the following: The $TiCl_4$ reaction with the Si(001) surface is strongly endothermic (i.e., it costs energy), 1.30 eV, but the kinetic barrier required to detach the hydrogen atom that passivates the Si dangling bond is relatively low compared with the energy of the chemisorbed configuration, 1.50 eV. The main reaction

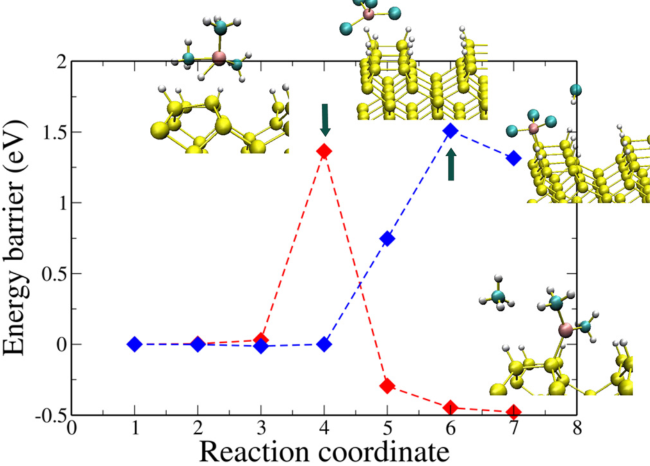


Fig. 1. (Color online) Kinetic energy barrier for the first adsorption step of TMA and $TiCl_4$ molecular precursors (red and blue curves, respectively) on a hydrogen-passivated Si(001)-(2×1) surface. The inset pictures show the transition and the final adsorption states for both molecules. Color code: small spheres represent hydrogen atoms, and Cl and C atoms surround the transition metals (Ti and Al, respectively). The arrows mark the transition states.

product is a Si:$TiCl_3$ bond and the loss of a HCl molecule. That small difference (0.20 eV) seems to indicate that there is a very low barrier for the readsorption of the HCl molecule and the detachment of the $TiCl_4$ precursor. These results agree relatively well with previous calculations using a cluster model (1.11 and 1.70 eV for the energy of the chemisorbed state and the kinetic barrier, respectively).[26]

Contrary to the $TiCl_4$ deposition onto the hydrogen-passivated Si(001)-(2×1) surface, the TMA chemisorption is slightly exothermic, −0.47 eV (a similar result of −0.39 eV was obtained using a surface cluster model and a different DFT exchange-correlation functional than the PBE functional used in our calculations[12]). The kinetic barrier for the chemisorption is also lower, 1.36 eV. The reason for this

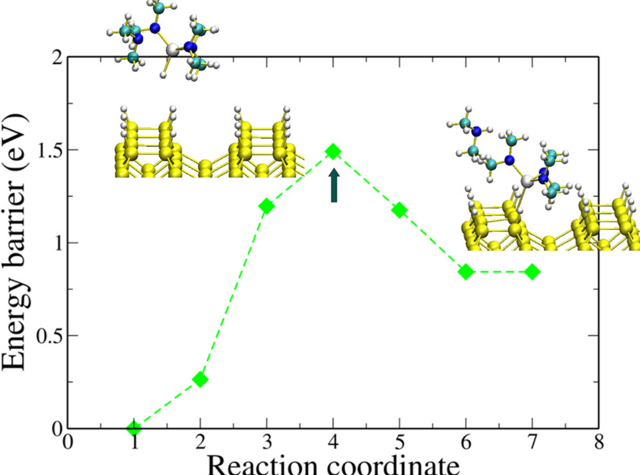


Fig. 2. (Color online) Kinetic energy barrier for the first adsorption step of the TDMA-Hf molecular precursor on a hydrogen-passivated Si(001)-(2×1) surface. The inset pictures show the transition and the final adsorption states. Color code: small spheres represent hydrogen atoms. In the molecule, the N atoms link the Hf atom (at the center) to the $CH_3$ groups. The arrows mark the transition states.

difference is twofold: First, the strong polarity of the HCl molecule (reaction product of the $TiCl_4$ deposition) makes the barrier for the H detachment much lower with respect to the final adsorption energy (0.20 eV). Second, the reaction product of the TMA deposition is the loss of a $CH_4$ molecule and the chemisorption of a $Al(CH_3)_2$ group, with the Al bonded to a Si surface atom. The energy gain of this reaction is noticeable, and as a consequence, there is a very high kinetic barrier (1.83 eV) for the readsorption of the methane molecule, indicating the much lower degree of selectivity of the TMA molecule, as compared to the $TiCl_4$ ALD precursor.

The ALD deposition of the TDMA-Hf molecular precursor is much more complex, especially due to the size of the molecule (37 atoms), which increases the number of degrees of freedom that need to be considered in the calculations. In this work, we have considered the initial reaction of the chemisorption of a $Hf[N(CH_3)_2]_3$ and the loss of a $HN(CH_3)_2$ reaction product, as shown in Fig. 2. The first consideration is that this reaction is slightly endothermic, as in the case of the $TiCl_4$ precursor but, with a much lower energy requirement, 0.84 eV, which also indicates a lower degree of selectivity. The kinetic barrier is also lower, 1.45 eV. The reason for these differences in the exo-/endothermic character of the chemisorption process is related to the metal-Si bond distance: 2.84, 2.48, and 2.68 Å for Hf-, Al- and Ti-Si, respectively. Although the kinetic barrier and the reaction energy of the chemisorbed configuration are relatively low compared to those of the $TiCl_4$ adsorption process, the size of the molecule seems to indicate that much better adsorption rates could be obtained in the presence of small surface defects, like Si dangling bonds or surface step edges.

If we consider a previous oxygen molecular precursor ALD cycle ($H_2O$ in our work), the hydrogen-passivated Si(001) surface will contain some OH surface species, providing a more chemically reactive environment for the chemisorption of the different molecular precursors. In our calculations, we have considered the dissociation of two $H_2O$ molecules on two neighboring Si dimers. Thus, two Si dimers of the hydrogen-passivated Si(001) surface are now OH-terminated. For the purpose of this work (to show the early stages of TMA, TDMA-Hf, and $TiCl_4$ chemisorption),

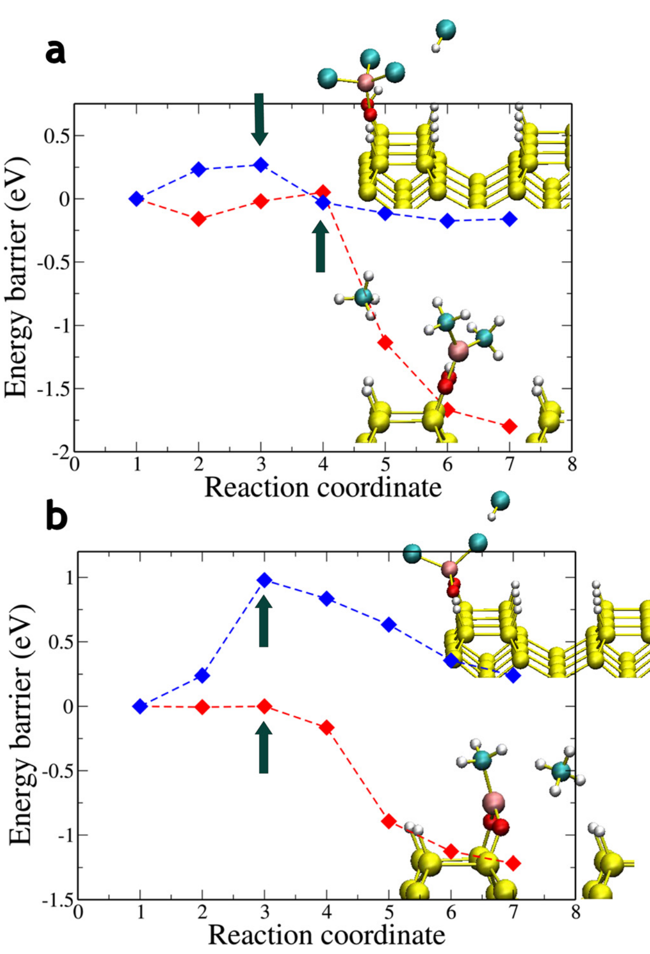


Fig. 3. (Color online) Kinetic energy barrier for the first adsorption step (a) and ring-closing reaction (b) of TMA and $TiCl_4$ molecular precursors (red and blue curves, respectively) on a OH-terminated Si(001)-(2×1) surface. The inset pictures show the final adsorption states for both molecules. Color code: small spheres represent hydrogen atoms, and Cl and C atoms surround the transition metals (Ti and Al, respectively). The arrows mark the transition states.

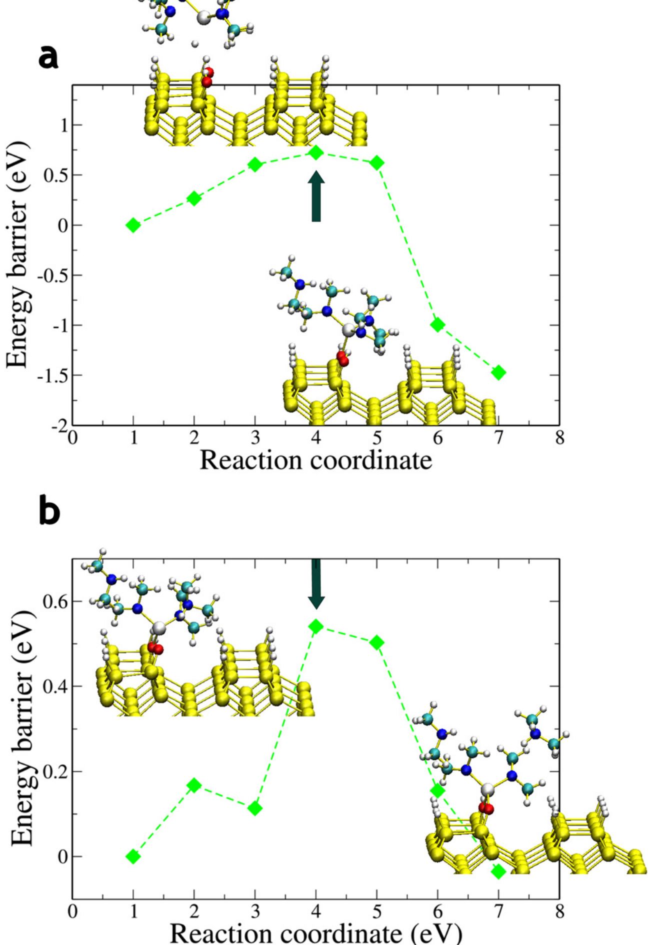


Fig. 4. (Color online) Kinetic energy barrier for the first adsorption step (a) and ring-closing reaction (b) of the TDMA-Hf molecular precursor on a OH-terminated Si(001)-(2×1) surface. The inset pictures show the final adsorption states. Color code: small spheres represent hydrogen atoms. In the molecule, the N atoms link the Hf atom (at the center) to the $CH_3$ groups. The arrows mark the transition states.

the increase of the oxygen rate deposition (OH surface species concentration) will not affect our main conclusions.

Figure 3(a) shows the reaction path of the TMA and $TiCl_4$ deposition on the hydrogen-passivated Si(001) surface with an OH termination in two neighboring dimers, and Fig. 4(a) shows the corresponding reaction pathway for the TDMA-Hf molecular precursor. Similarly to the hydrogen-terminated Si(001) surface, the chemisorption of the TMA releases a methane $CH_4$ molecule and the deposition of the $TiCl_4$ releases a polar HCl molecule. The Coulomb attraction between the molecular precursor and the negatively charged OH surface species decreases the kinetic barriers substantially, as it can be seen in Fig. 3(a). The kinetic barrier for the TMA molecule is only 0.05 eV, whereas the $TiCl_4$ molecular precursor kinetic chemisorption barrier is slightly larger, 0.26 eV. However, the main difference lies in the reaction energies. Both pathways are exothermic, but the TMA chemisorption energy is 1.79 eV, whereas the $TiCl_4$ reaction energy is only 0.15 eV. This means that the desorption kinetic barrier of the $TiCl_4$ molecule (or readsorption of the released HCl) is only 0.41 eV, much lower than the 1.84 eV desorption barrier for the TMA precursor. The deposition of the TDMA-Hf molecule shows different features. As we pointed out earlier, the larger size of the molecule makes necessary to overcome a higher kinetic barrier to release an $HN(CH_3)_2$ group and form the O-Hf bond, because it has to exceed the strong steric repulsion with the surface and, as a consequence, the TDMA-Hf molecule is finally chemisorbed with a more planarlike configuration, compared to the initial three-dimensional (3-D) shape of the molecule. The Hf-O bond distance is 1.95 Å (cf. with 1.71 and 1.77 Å for Al-O and Ti-O distances, respectively). Then, our obtained kinetic barrier is the largest among the three precursors, 0.72 eV, but the reaction is again strongly endothermic [see Fig. 4(a)], 1.47 eV, indicating a much lower degree of selectivity, as compared to the $TiCl_4$ molecular precursor.

Finally, the neighboring OH surface species make possible a ring-closing reaction, with the formation of a double O-metal-O bond and the release of additional $CH_4$, HCl, or $HN(CH_3)_2$ molecules, for TMA, $TiCl_4$, and TDMA-Hf chemisorption, respectively. Figures 3(b) and 4(b) show the corresponding reaction pathways for the three molecular precursors. Similar considerations are in order: the kinetic barrier for the release of another methane $CH_4$ molecule is almost negligible, and the reaction is strongly exothermic, 1.21 eV. For the $TiCl_4$ precursor, the kinetic barrier is substantially higher, 0.97 eV, and the reaction is slightly endothermic, 0.23 eV. The Al atom has an empty 3*p* orbital, which is attracted to the $O^{2-}$ surface charged species much stronger than the $TiCl_3$ molecule, because of the negatively charged $Cl^-$ atoms. For the same considerations aforementioned, the kinetic barrier for the ring-closing reaction of the TDMA-Hf, with the release of another $HN(CH_3)_2$ molecule, is 0.54 eV, and the reaction is exothermic, but with a reaction energy of only 0.03 eV. The final O-metal bond distances are 1.73, 1.80, and 1.96 Å for Al, Ti, and Hf, respectively.

Figure 5 shows the Ti 2*p*, Al 2*p*, and Hf 4*f* core-level regions after atomic layer deposition of $TiO_2$, $Al_2O_3$, and $HfO_2$ on both hydrogen- and OH-terminated Si(001). It is clear that for the OH treated Si(001) surface, significant and predictable growth of all three metal oxidized is observed. However, for the hydrogen-terminated surfaces, the growth in all three cases is diminished. The high selectivity for the $TiCl_4/H_2O$ system shown in Fig. 5 (left panel) has been discussed in detail by Mc Donnell *et al.*[28] However, the selectivity observed for $TMA/H_2O$ and TMDA-Hf/$H_2O$ are both significantly less than the $TiCl_4/H_2O$ system. Instead, the Al 2*p* and Hf 4*f* intensities for the hydrogen-terminated Si(001) surface are 38% and 75% of the those observed on OH-terminated Si(001).

## B. Discussion

The adsorption mechanisms found in our DFT calculations for $TiCl_4$, TMA, and TDMA-Hf molecular precursors on the OH- and hydrogen-terminated Si(001) surfaces clearly explain the different degree of selectivity found in our XPS measurements. Indeed, Fig. 5 shows that there is no detectable $TiO_2$ signal in a hydrogen-terminated Si(001) surface, whereas for $Al_2O_3$ the signal in a hydrogen-terminated

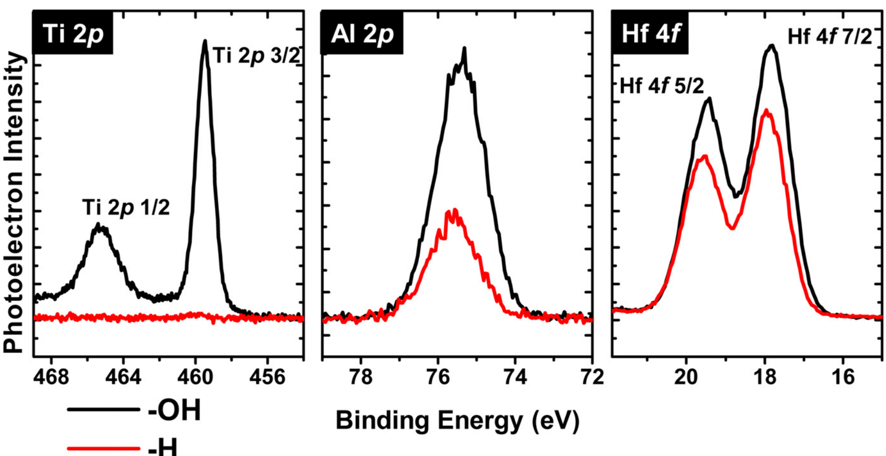


FIG. 5. (Color online) Ti 2*p*, Al 2*p*, and Hf 4*f* after 10 cycles of $TiCl_4/H_2O$, $TMA/H_2O$, and TDMA-Hf/$H_2O$, respectively, on OH- (upper curves) and hydrogen terminated (lower curves) Si(001) surfaces. The three spectra correspond to depositions at 150 °C.

Si(001) surface is 38% of the OH-terminated signal. Finally, for $HfO_2$, the rate increases up to 75%. Although the high selectivity found in our experiments for $TiO_2$ is larger than that previously reported,[44] the trends observed are consistent with the kinetic barriers and the degree of exo-/endothermicity obtained for the different deposition reactions: in a hydrogen-terminated Si(001) surface, the three molecular precursors show (relatively) high kinetic barriers (around 1.5 eV), but the $TiCl_3$ chemisorption (with the release of a HCl polar molecule) is the most endothermic reaction (1.30 eV) among all the processes studied in this work (cf. with −0.47 and 0.84 eV for TMA and TDMA-Hf molecular precursors, respectively). On the contrary, on an oxidized Si(001) surface, the high chemical reactivity of the oxygen lone pair significantly decreases the kinetic barriers required to release the different reaction products (HCl, $CH_4$, and $HN(CH_3)_2$, respectively, for TiCl4, TMA, and TDMA-Hf ALD pulses) and the formation of the Si-O-metal bond. The reaction energies, however, follow the same trend as in the hydrogen-terminated Si(001) surface: strongly exothermic for TMA and TDMA-Hf molecular precursors (1.79 and 1.47 eV, respectively) and practically negligible for $TiCl_4$ (0.15 eV). The reason, again, is purely electrostatic. The Coulombic repulsion between the surface $O^{2-}$ and the $Cl^-$ ions of the $TiCl_4$ molecular precursor makes the ALD growth of $TiO_2$ more selective and less favorable, when compared with $Al_2O_3$ and $HfO_2$.

## V. SUMMARY AND CONCLUSIONS

In conclusion, we have investigated the energetics and the kinetic barriers of the early adsorption steps of three different molecular precursors ($TiCl_4$, TMA, and TDMA-Hf) onto the OH- and hydrogen-terminated Si(001)-(2×1) surfaces for ALD experiments of metal-oxide growth on Si surfaces. While the higher kinetic barrier and endothermic character corresponds to the chemisorption of a $TiCl_3$ group and the loss of a polar HCl molecule ($TiCl_4$ deposition), the adsorption of the Al is a very favorable process due to the loss of a methane molecule, which strongly contributes to stabilize the system. Similar considerations arise for the Hf chemisorption [and the loss of a $HN(CH_3)_2$ group]. These facts seem to indicate that the $TiCl_4$ molecule shows the larger degree of selectivity among all the molecular precursors studied in this work, as further confirmed by the XPS spectra obtained after the ALD growth of $TiO_2$, $Al_2O_3$, and $HfO_2$ high-$\kappa$ dielectric materials.

## ACKNOWLEDGMENTS

This work was supported by the Defense Advanced Research Project Agency (DARPA) and Space and Naval Warfare Center, San Diego (SPAWARSYSCEN-SD) under contract N66001-08-C-2040. It was also supported by a grant from the Emerging Technology Fund of the State of Texas to the Atomically Precise Manufacturing Consortium. The calculations were performed in the Texas Advanced Computing Center (TACC).

[1]G. E. Moore, "Progress in digital integrated electronics," *Proceedings of the International Electron Devices Meeting (IEDM'75)* (1975), Vol. 21, pp. 11–13.
[2]P. A. Packan, Science **285**, 2079 (1999).
[3]*Semiconductor Industry Association, The National Technology Roadmap for Semiconductors: Technology Needs*, 1997 ed. (SEMATECH, Austin, TX, 1997).
[4]S. M. George, A. W. Ott, and J. W. Klaus, J. Phys. Chem. **100**, 13121 (1996).
[5]E. P. Gusev, M. Copel, E. Cartier, I. J. R. Baumvol, C. Krug, and M. A. Gribelyuk, Appl. Phys. Lett. **76**, 176 (2000).
[6]M. Copel, M. A. Gribelyuk, and E. P. Gusev, Appl. Phys. Lett. **76**, 436 (2000).
[7]M. L. Green *et al.*, J. Appl. Phys. **92**, 7168 (2002).
[8]E. P. Gusev, C. Cabral, Jr., M. Copel, C. D'Emic, and M. A. Gribelyuk, Microelectron. Eng. **69**, 145 (2003).
[9]W.-H. Kim, H.-B.-R. Lee, K. Heo, Y. K. Lee, T.-M. Chung, C. G. Kim, S. Hong, J. Heo, and H. Kim, J. Electrochem. Soc. **158**, D1 (2011).
[10]H.-B.-R. Lee and H. Kim, ECS Trans. **16**, 219 (2008).
[11]H.-B.-R. Lee, W.-H. Kim, J. W. Lee, J.-M. Kim, K. Heo, I. C. Hwang, Y. Park, S. Hong, and H. Kim, J. Electrochem. Soc. **157**, D10 (2010).
[12]M. D. Halls and K. Raghavachari, J. Chem. Phys. **118**, 10221 (2003).
[13]M. D. Halls and K. Raghavachari, J. Phys. Chem. B **108**, 4058 (2004).
[14]Y. Widjaja and C. B. Musgrave, Appl. Phys. Lett. **80**, 3304 (2002).
[15]D.-H. Kim, S. B. Baek, and Y.-H. Kim, Appl. Surf. Sci. **258**, 225 (2011).
[16]M. K. Ghosh and C. H. Choi, Chem. Phys. Lett. **426**, 365 (2006).
[17]M. K. Ghosh and C. H. Choi, J. Phys. Chem. B **110**, 11277 (2006).
[18]A. Heyman and C. B. Musgrave, J. Phys. Chem. B **108**, 5718 (2004).
[19]Y. Widjaja, J. H. Han, and C. B. Musgrave, J. Phys. Chem. B **107**, 9319 (2003).
[20]Y. Widjaja and C. B. Musgrave, Appl. Phys. Lett. **81**, 304 (2002).
[21]L. Jeloaica, A. Estève, M. D. Rouhani, and D. Estève, Appl. Phys. Lett. **83**, 542 (2003).
[22]Y. Xu and C. B. Musgrave, Chem. Mater. **16**, 646 (2004).
[23]M. D. Halls and K. Raghavachari, J. Phys. Chem. A **108**, 2982 (2004).
[24]Z. Hu and C. H. Turner, J. Phys. Chem. B **110**, 8337 (2006).
[25]Z. Hu and C. H. Turner, J. Am. Chem. Soc. **129**, 3863 (2007).
[26]M. K. Ghosh and C. H. Choi, Chem. Phys. Lett. **461**, 249 (2008).
[27]M. K. Ghosh and C. H. Choi, Chem. Phys. Lett. **457**, 69 (2008).
[28]S. McDonnell *et al.*, J. Phys. Chem. C **117**, 20250 (2013).
[29]A. Zydor, S. D. Elliott, T. Leese, F. Song, and S. Rushworth, ECS Trans. **11**, 113 (2007).
[30]K. Black *et al.*, J. Mater. Chem. **18**, 4561 (2008).
[31]A. Zydor and S. D. Elliott, J. Phys. Chem. A **114**, 1879 (2010).
[32]M. Shirazi and S. D. Elliott, J. Comp. Chem. **35**, 244 (2014).
[33]G. Kresse and J. Hafner, Phys. Rev. B **47**, 558 (1993).
[34]G. Kresse and J. Furthmüller, J. Comput. Mater. Sci. **6**, 15 (1996).
[35]J. P. Perdew, K. Burke, and M. Ernzerhof, Phys. Rev. Lett. **77**, 3865 (1996).
[36]H. Jónsson, G. Mills, and K. W. Jacobsen, in *Classical and Quantum Dynamics in Condensed Phase Simulations*, edited by B. J. Berne, G. Ciccotti, and D. F. Coker (World Scientific, Singapore, 1998), pp. 385–404.
[37]G. Henkelman and H. Jónsson, J. Chem. Phys. **113**, 9978 (2000).
[38]G. Henkelman, B. P. Uberuaga, and H. Jónsson, J. Chem. Phys. **113**, 9901 (2000).
[39]H. K. Monkhorst and J. D. Pack, Phys. Rev. B **13**, 5188 (1976).
[40]R. M. Wallace, ECS Trans. **16**, 255 (2008).
[41]P. Sivasubramani, J. Kim, M. J. Kim, B. E. Gnade, and R. M. Wallace, J. Appl. Phys. **101**, 114108 (2007).
[42]A. Pirkle, S. McDonnell, B. Lee, J. Kim, L. Colombo, and R. M. Wallace, Appl. Phys. Lett. **97**, 082901 (2010).
[43]A. Herrera-Gomez, A. Hegedus, and P. L. Meissner, Appl. Phys. Lett. **81**, 1014 (2002).
[44]R. Methaapanon and S. F. Bent, J. Phys. Chem. C **114**, 10498 (2010).